Фізика аеродисперсних систем. – 2025. – № 63. – С.127-135

ГАЗОДИНАМІКА

UDC 533.9,524.1

Doikov D. N.[1], Doikov M. D.[2]

[1] Dept. of Physics, Medical Laboratory, Northern Medical Center, Poria, Israel
dmitro.doikov@gmail.com
[2] Faculty of Physics and Technology, Plovdiv University "Paisii Hilendarski", Plovdiv, Bulgaria
marik.doikov@gmail.com
ORCID: [1] https://orcid.org/0000-0002-6965-3662
[2] https://orcid.org/0000-0002-7029-8397

Analysis of atmospheric aerosol contamination under thunderstorm conditions

This work investigates the feasibility of using lightning discharges as a natural high-energy radiation source for atmospheric sounding. Based on the typical energy distribution of lightning self-radiation, radiative transfer through cloud aerosols composed of water vapor and pollutant particles — such as quartz, sodium chloride, and soil-derived organic matter — was modeled. Scattering indicatrices x(θ) for X-ray and gamma radiation were calculated. Solutions to the radiative transfer equation were compared under both single and multiple scattering approximations. For the first time, a spectroscopic method is proposed for identifying aerosol properties based on singly scattered radiation spectra.

Keywords*: hard radiation detectors, lightning, radiation deposition, X-ray diagnostic of dirty transparent windows, diffusion emission, thunderstorm aerosol.*

Introduction. Lightning discharges occurring during both meteorological thunderstorms and volcanic eruptions generate broadband electromagnetic radiation, ranging from radio frequencies to gamma rays. A significant portion of the high-energy photon emission arises from bremsstrahlung and characteristic radiation produced in the intense electric fields near the discharge channel, where atmospheric gas ions are highly energized.

The characteristic X-ray lines predominantly lie in the soft X-ray region and are subject to strong photoabsorption in the dense plasma surrounding the discharge channel. This plasma region primarily contains ions of nitrogen, oxygen, and carbon, along with other trace elements. In the case of volcanic plumes, additional emission lines emerge, corresponding to species such as silicon (Si), sulfur (S), and phosphorus (P), which are commonly present in volcanic ejecta.

Detection of higher-energy photons provides enhanced capability for probing the near-discharge region, owing to their lower attenuation coefficients in aerosol-laden media. As these photons propagate outward, they undergo energy loss via photoabsorption, inelastic Compton scattering, and elastic Rayleigh scattering. For pure water aerosols, cross-sectional ratios for these processes were previously derived and presented in [5, Fig. 2]. However, in realistic scenarios involving mixed or polluted aero-

DOI: 10.18524/0367-1631.2025.63.347245

sols, the spectral and angular characteristics of scattered radiation can differ significantly.

The present study investigates X-ray and gamma-ray scattering in both pure and contaminated aerosol media, including constituents such as quartz, salt, and soil-derived organics. Scattering indicatrices and spectral transformations were modeled and analyzed under various conditions relevant to atmospheric and volcanic discharges.

This paper is organized as follows: Section 2 examines the formation and characteristics of high-energy radiation in atmospheric lightning events. Section 3 addresses discharge dynamics and radiative emissions in volcanic cloud plumes. Section 4 presents a spectroscopic analysis of scattered X-ray radiation in liquid and aerosol environments. The Discussion outlines implications for remote sensing and introduces a novel diagnostic approach based on single-scattering spectra. The Conclusion summarizes the key findings and highlights potential applications in aerosol composition analysis.

1. Polluted Aerosols in Thunderstorm Clouds. Lightning activity in thunderstorm clouds has been the subject of scientific inquiry for over three centuries and remains a central topic in atmospheric research. The aerosol phase of thunderclouds comprises both a dispersed component (liquid droplets and ice particles) and a gaseous phase consisting of water vapor mixed with air. The fundamental physical characteristics and dynamics of lightning development are addressed in detail in studies such as [1, 2, 6, 10].

In this study, we define "polluted" or "dirty" aerosols as droplets containing micron-scale inclusions of solid particles. The optical properties of such aerosols have been extensively investigated within meteorology and plasma electrodynamics over the past several decades. Radiative transfer modeling through cloud structures of this type requires prior knowledge of the scattering indicatrix $X(\theta)$, which governs the angular distribution of scattered photons. The choice of radiative transfer approximation - whether single or multiple scattering - depends on the physical assumptions and specific configuration of the aerosol components. Here, we consider various pollutant compositions: solid particles embedded in droplets, dissolved contaminants, or combinations thereof. Traditional diagnostic approaches in the optical spectral range rely on macroscopic aerosol parameters and often require accounting for multiple scattering events. These methods have led to significant theoretical and practical advancements in the field over the past 60 years [5].

In clean cloud systems, Rayleigh scattering by water molecules typically dominates the visible and near-infrared spectral domains. However, the introduction of impurities substantially alters both are provocated by the scattering and absorption characteristics of solar radiation [10, 11]. X-ray and gamma-ray spectroscopy of thunderstorm clouds offers complementary diagnostic capabilities [3, 4]. Advances in spectroscopic instrumentation now enable the detection of high-energy photon interactions with individual atoms in polluted aerosols, with lightning discharges themselves serving as transient radiation sources. Previously, we analyzed the detector configuration and simulated its response in photon-counting mode.

In this work, millisecond- and microsecond-scale bursts of X-ray and gamma

radiation emitted during lightning events are utilized to probe aerosol composition. As shown in [7, 8], certain energy intervals exist where photoabsorption is significantly weaker than inelastic Compton scattering. Accurate spectral diagnostics are achievable under conditions dominated by single-scattering events.

The Compton scattering process is governed by the photon–electron interaction cross section [8, Fig. 7, 8] and the scattering indicatrix X(θ), which is described by the Klein–Nishina formula for angular distribution of scattered photons.

$$\frac{d\sigma}{d\Omega} = \frac{r_0^2}{2}\left(\frac{E'}{E}\right)^2\left(\frac{E'}{E} + \frac{E}{E'} - sin\theta\right). \quad (1)$$

Here, θ denotes the scattering angle with respect to the incident photon direction; E and E′ represent the energies of the incident and scattered photons, respectively; r_0 is the classical electron radius; Ω is the solid angle subtended at the point of interaction, corresponding to the conical volume encompassing the detector's active area.

By combining the Compton equation with the Klein–Nishina formula into a unified system, one can describe both the energy and angular characteristics of inelastic photon scattering on free electrons.

$$\begin{cases} \lambda' - \lambda = 2.43 \cdot 10^{-3}(1 - \cos\theta) \\ E'_\gamma = \dfrac{E_\gamma}{1 + (E_\gamma / 511)(1 - \cos\theta)} \end{cases} \quad (2)$$

We derive the scattering indicatrix $x(\theta)$;which characterizes the angular distribution of the scattered radiation intensity

$$x(\theta) = \frac{E'_\gamma}{E_\gamma} = \frac{1}{1+(E_\gamma/511)(1-\cos\theta)}. \quad (4)$$

The probability of photon emission at an angle θ relative to the incident direction, for a known angular distribution function $x(\theta)$, is given by the following equation:

$$dP_{E_\gamma}(\theta) = x(\theta)\frac{d\omega}{4\pi} = \frac{1}{1+(E_\gamma/511)(1-\cos\theta)} \cdot \frac{d\omega}{4\pi} = \frac{1}{1+(E_\gamma/511)(1-\cos\theta)} \frac{\sin\theta d\theta}{2}. \quad (5)$$

After integration over dθ, the final expression for the total probability $P_{E_\gamma}(\theta)$ is obtained:

$$P_{E_\gamma}(\theta) = \frac{511}{E_\gamma} ln\left|1 + (2E_\gamma/511)\right| \quad (6)$$

The scattering indicatrix $x(\theta)$ can conveniently be represented in a Cartesian coordinate system along the X and Y axes, with components defined by the directional intensities of scattered radiation $I(\theta)$ as a function of angle θ. This representation is particularly suitable for use in equation (1).

$$X = I(\theta)\cos\theta;\ Y = I(\theta)\sin\theta \quad (7)$$

The radiation intensity $I(\theta)$ is governed by the scattering indicatrix x(θ) and the cross sections of elementary absorption and scattering processes. All major cross sections relevant to these interactions are presented in [Fig. 1]. Analysis of this figure indicates that the "transparency window" approximation for X-ray emissions generated by lightning becomes valid for photon energies of $E_\gamma \geq 40\ keV$.

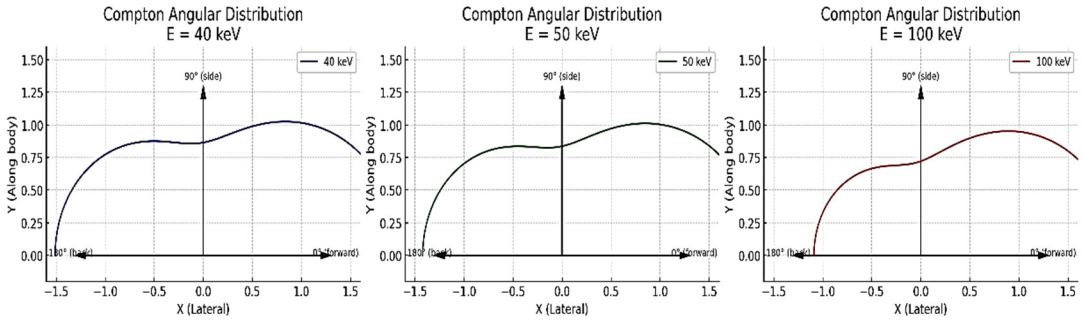

Fig. 1. Angular distribution diagrams of the scattered radiation intensity $I(\theta)$ in a "pure water" medium. The X and Y axes are defined according to equation (7). Results are shown for incident photon energies). E_γ=40, 50 и 100 keV.

Accordingly, we present computed angular intensity distributions $I(\theta)$ incorporating the scattering behavior described by $x(\theta)$, for incident photon energies of 40, 50, and 100 keV. As shown in [8], Compton scattering dominates in this energy range.

As shown in Fig.1, in a "pure water" medium, the spatial distribution of scattered photons becomes increasingly isotropic as the energy of the incident X-ray beam increases to $E_\gamma \geq 40\ keV$. To evaluate the effects of contamination, we consider the presence of both solid inclusions and dissolved pollutants. The hypothetical contaminant is assumed to consist of two components: an insoluble (solid) fraction and a soluble fraction. The primary scattering agents are represented as fractions composed of various particle types, as detailed in Table 1.

The solid fraction of atmospheric dust is modeled as a mixture of multiple subfractions, each following a log-normal particle size distribution.

$$\frac{dN}{dlgd} = \frac{N_0}{\sqrt{2\pi} lg\sigma_g} exp\left[-\frac{(lgd-lgd_g)^2}{2(lg\sigma_g)^2}\right]. \quad (8)$$

Here, $\frac{dN}{dlgd}$ denotes the number of particles within a logarithmic diameter interval; N_0 is the normalization factor representing the total number of particles per unit volume; d_g is the geometric mean particle size. The planned experimental sites include the region of Smolyan (Bulgaria), characterized by significant concentrations of Na^+ and Cl^-, and the Catania region near Mount Etna (Sicily, Italy), where aerosols commonly contain Mg^{2+}, K^+, SO_4^{2-}, Na^+, and Cl^-. According to Table 1, the typical mass fractions for these aerosol impurities are 5–20% and 2–5% for the respective regions. The scattering properties of aerosols enriched with these components depend on both their mass fraction and the atomic number Z of the constituent elements. Higher average atomic numbers and greater mass fractions result in more pronounced energy differences in the scattered spectrum, within the X-ray "transparency windows" utilized in this study. The contribution of X-ray diffraction by nanoparticles was previously discussed in [3, 4]. However, under realistic atmospheric conditions, diffraction-based scattering halos are expected to occur only in the immediate vicinity of cloud structures. The relative contribution of Compton scattering on atoms versus diffraction on nanoscale particles is governed by the number of scatterers, their atomic number Z, and the number density of nanoparticles within the irradiated volume. As

shown in [3], the contribution of diffraction to the overall X-ray scattering is

Table 1. Impurity components and localization of atmospheric aerosols

n/n	Component	Mass fraction	Primary source(s)
1	SiO_2	15–25%	Saharan dust (mineral origin)
2	Al_2O_3	3–7%	Mineral dust
3	$CaCO_3$ / Ca^{2+}	5–15%	Soil dust, limestone, construction materials
4	Fe_2O_3 / Fe^{3+}	2–6%	Desert dust
5	Na^+, Cl^-	5–20% (higher near coast)	Marine aerosols
6	Mg^{2+}, K^+, SO_4^{2-} Na^+, Cl^-	2–5%	Marine aerosols + volcanic emissions
7	NO_3^-, NH_4^+	3–10%	Traffic emissions, fertilizers
8	Black carbon (soot)	2–8%	Diesel vehicles, biomass burning
9	Organic compounds	5–15%	Biomass, urban smog
10	Pb, Zn, Cu, Cr, Ni	<1%	Traffic, metallurgy, brake and tire wear

significantly lower than that of atomic interactions, particularly in the hard X-ray regime.

2. Volcanic Environments. During eruptions of most volcanoes, eruptive emissions consist of approximately 95% water vapor, along with volcanic ash containing various solid mineral particles. Calculations for quartz particles with mean sizes ranging from 1 μm to 0.1 mm, as presented in Fig. 3, indicate that at photon energies $E_\gamma \geq 40\ keV$, the probability of photoabsorption becomes comparable to or lower than that of Compton and Rayleigh scattering. Fig. 3 shows the probabilities of all major photon interaction processes in water at an equivalent thickness of 200 mm. During an eruption, water on the surface of solid particles evaporates almost instantly, forming a cloud composed of superheated vapor and suspended solid matter.

For nanoscale quartz particles, additional simulations were carried out (see Fig. 4), evaluating interaction probabilities and highlighting the role of scattering mechanisms at small particle sizes. In addition for sensitive detectors we have possibility to observe soft X- and hard UV-rays diffraction. The macroscopic electrodynamic parameters are considered in [3, 4]. From diffraction in 2D-imagion has been observed X-ray Galo around point X-ray sources in space. The hard X-ray emission produced by lightning discharges near volcanic plumes is inherently pulsed, with pulse durations on the order of milliseconds. Consequently, detection of such emissions requires spectrometers operating in microsecond resolution mode [8,9]. As the effective number of scattering particles between the lightning source and observer increases, the role of multiple scattering becomes more pronounced. Modeling this regime involves tracking the full photon trajectory geometry through a medium composed of randomly distributed solid particles.

Fig. 3 presents the simulation results for distilled water, while Fig. 4 corresponds

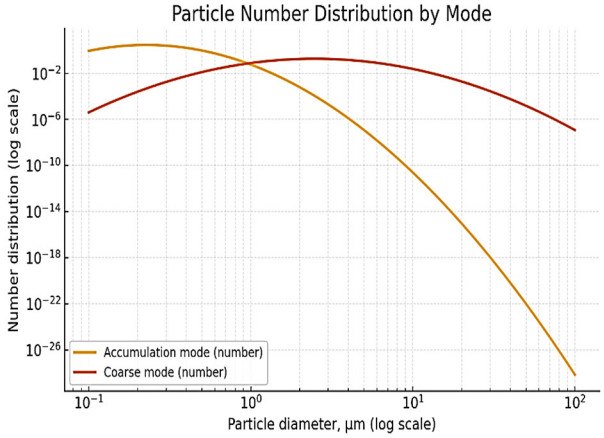

Fig. 2. Size distribution of aerosol particles expressed as $\frac{dN}{dlgd}$ as a function of particle diameter d.

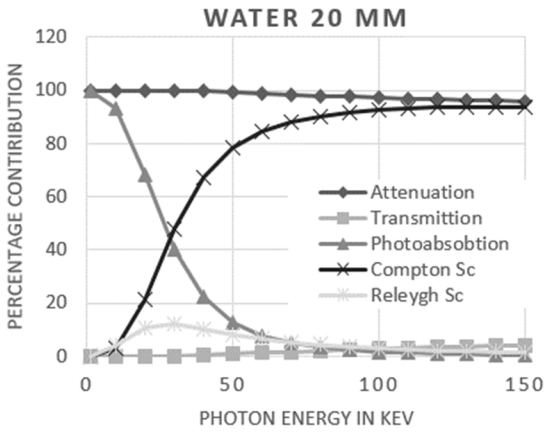

Fig 3. Simulation results for distilled water

to quartz (SiO_2). The modeling is based on the Monte Carlo method, which accounts for the stochastic nature of elementary photon interactions with atoms and their electrons. In the first approximation, the radiation transport is considered primarily as a function of the effective atomic number. This approach is justified by the fact that, at photon energies $E_\gamma \geq 40\ keV$ the surrounding atmosphere becomes a transparency window, exerting minimal distortion on the signal originating from the volcanic cloud.

X-ray spectroscopy of polluted dispersed aerosols triggered by lightning flashes offers new opportunities for identifying the chemical composition of contaminants based on the ratio of absorbed to scattered radiation. The probability of detecting characteristic radiation is negligible in the energy range $0.1\ keV \leq E_\gamma \leq 40\ keV$ due to strong photoabsorption. Compton scattering is the dominant mechanism for both single and multiple scattering events in polluted aerosols, with Rayleigh scattering contributing to a lesser extent across all typical impurity elements. Defining transparency windows in the medium enables the identification of conditions under which single Compton scattering dominates. This criterion is crucial for analyzing any aerosol system - regardless of its contamination level - when it lies along the propagation path of hard X-ray photons emitted by lightning toward the detector.

3. Laboratory Simulation. For the laboratory investigation of hard X-ray scattering by polluted aerosols, we propose using a standard X-ray tube in combination with open-source simulation tools based on the Geant4-DNA framework [7,9]. This approach offers simplicity, reproducibility, and accessibility. As model scatterers representing aerosol contaminants, we consider quartz particles and barium sulfate ($BaSO_4$), the latter being widely used in medical imaging and exhibiting well-characterized log-normal size distributions.

To conduct both numerical and subsequent physical experiments, it is necessary to define the energy range and particle size regime where single scattering events are most probable.The experimental geometry consists of a "transparent" aerosol-containing cylinder aligned along the Y-axis. In the X–Y plane, at a distance of 0.5 m

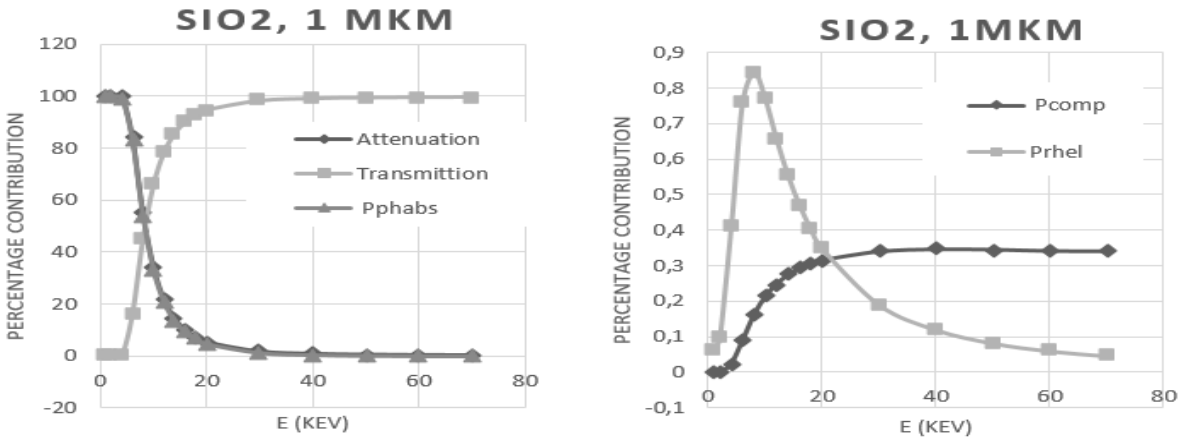

Fig. 4. Percentage contribution of major interaction processes for X-ray photons in quartz (SiO_2) particles: total attenuation, photoabsorption P_{abs}, transmission, Compton scattering P_{comp}), and Rayleigh scattering P_{rhel}

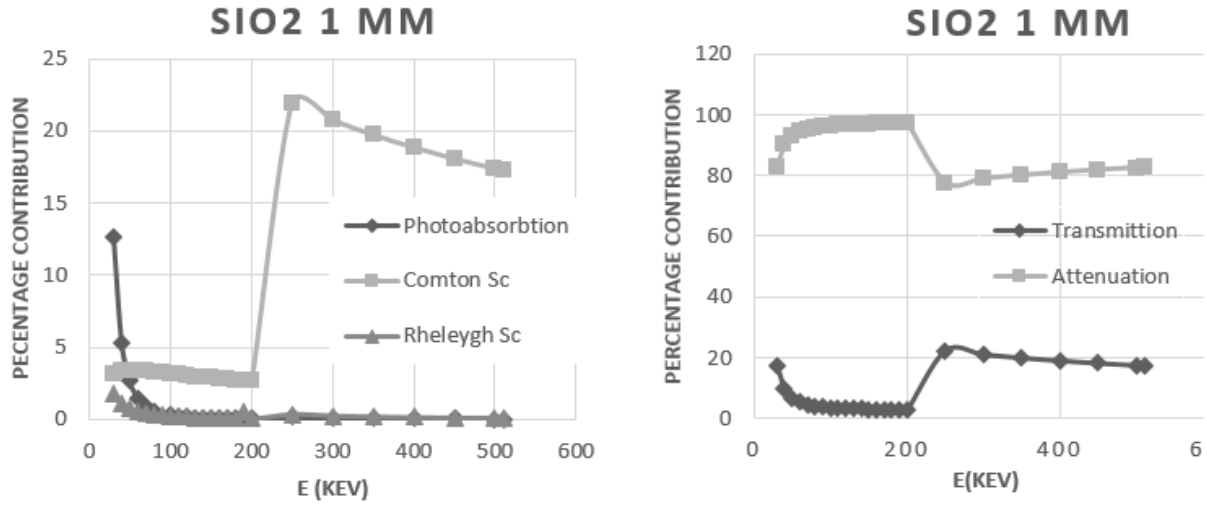

Fig. 5. Corresponding distribution for silicon dioxide (SiO_2) particles with a thickness of 1 mm

from the cylinder center, a circular array of $CsPbBr_3$ detectors is positioned. Each detector has a volume of 1 cm^3, sufficient to fully absorb incident X-rays within a 1–2 mm active layer, enabling high-efficiency spectral detection and angular resolution. This configuration yields the angular distribution of scattered radiation intensity as a function of detector position. After normalization, the numerical scattering indicatrix x(θ) is obtained. The measured data are compared with results from numerical simulations performed using Geant4-DNA. The modeling setup and results of the computational experiment are presented in Fig. 5.

4. Discussion. The growing demand for cost-effective third-generation hard radiation spectrographic detectors is driven by their significant advantages, primarily due to the use of new-generation semiconductors incorporating elements with high average atomic numbers Z. The cross sections and probabilities of the fundamental processes of photon absorption and scattering strongly depend on various powers of Z, thereby

enabling new capabilities for hard radiation spectral detection with microsecond time resolution. At photon energies $E_\gamma \geq 40\ keV$, the detected spectra can be unambiguously correlated with the presence of specific contaminant aerosol atoms. However, solving such problems requires dedicated electronic interfaces capable of operating in standby mode and performing active rejection of irrelevant data [9].

Conclusion. This study investigates the X-ray and gamma-ray spectra produced by lightning activity in thunderstorm clouds and volcanic plumes. Energy intervals and particle concentrations were identified under which single and multiple scattering approximations for X-ray photons are valid. In the case of single scattering, the scattering indicatrix x(θ) was derived, and the radiative transfer equation was solved for various media to determine the angular intensity distribution I(θ) of the scattered radiation. For multiple scattering regimes, statistical modeling approaches were applied using Monte Carlo methods implemented in the Geant4-DNA framework (version 11.3.2) [10]. Both methods demonstrated sensitivity to the atomic and chemical composition of the medium and were employed to derive quantitative characteristics of pollutant components in dispersed aerosols within thunderstorm clouds and volcanic emissions, including assessments of their spatial stratification.

References:

1. *Frank S. Marzano, Luigi Mereu, Simona Scollo[...], Costanza Bonadonna.* Tephra mass eruption rate from ground-based X-band and L-band microwave radars during the November 23, 2013, Etna paroxysm. IEEE Transactions on Geoscience and Remote Sensing. 2020. Vol. 58, no. 5. P. 3314–3327.
2. *Cimarelli,Genareau K.* Review of volcanic electrification of the atmosphere and volcanic lightning // Journal of Volcanology and Geothermal Research. Invited review article. – 2022. – Vol. 422. Article 107449.
3. *B.T. Draine //* Astrophys. J. – 2016. – 831, 109 (19 pp)
4. *Weingarter J. C., Draine B.T., Barr D.K.* //Astrophys. J., 2006, 645; 1188.
5. *Mischenko M.I., J.W. Hovenier., D.W.Mackowski* // J. Opt. Soc. Am. A. – 2004. – Vol. 21, 1. – P. 71–81.
6. *Козырев А.В., Тарасенко В.Ф., Бакшт Е.Х, Шутько Ю.В.* // Письма в ЖТФ. – 2011. – Т. 37, вып. 22. – С. 26–33.
7. *Weber G*. X-Ray attenuation & absorption calculator. https://web-docs.gsi.de/~stoe_exp/web_programs/x_ray_absorption/index.php
8. *Doikov, D. N., Doikov, M. D.* // Physics of aerodisperse systems. – 2024. – 62. – P. 111-119. DOI: 10.18524/0367-1631.2024.62.318610
9. *Doikov M.D.* // OAP. – 2022. – 35. – pp. 24-29. DOI 10.18524/1810-4215.2022.35.268000
10. *Incerti S., Baldachino G., Bernal M. et al.* // Int. J. of Modeling, Simulation, and Scientific Computing. – 2010. – Vol. 1, iss. 2. P. 157–178. https://doi.org/10.1142/S1793962310000122
11. *Gurevich A, V., K.P. Zybin.* // Usp. Phys. Nauk. 2001. Vol. 171, iss. 11. P. 1177–1199.
12. *Petrov N.I. //* Scientific Report. – 2021. – Vol. 11. Article 19824. https://doi.org/10.1038/s41598-021-99336-3

Фізика аеродисперсних систем. – 2025. – № 63. – С.127-135

Дойков Д. Н., Дойков М. Д.

Аналіз забруднення атмосфери аерозолями в умовах блискавок

АНОТАЦІЯ

У роботі здійснено спробу зондування атмосфери Землі шляхом реєстрації рентгенівських та гамма-спектрів, що випромінюються грозовими розрядами різних типів. На основі стандартного енергетичного розподілу власного випромінювання блискавок розглянуто перенесення випромінювання крізь хмарний аерозоль, який складається з водяних мікрокрапель та домішкових частинок кварцу, солей і ґрунтової органіки.

Отримано індикатриси розсіювання $\chi(\theta)$ *рентгенівського та гамма-випромінювання на аерозольних частинках. Виконано порівняльний аналіз результатів розв'язання рівняння перенесення випромінювання в наближеннях одноразового та багаторазового розсіювання у забруднених аерозолях. Вперше запропоновано метод діагностики досліджуваних об'єктів за спектрами одноразового розсіювання агентами забруднення.*

Показано, що навколо струмового циліндра існує розширена зона іонізованого аерозолю, в якій формується оптичне випромінювання. Зроблено висновок, що джерела рентгенівського та гамма-випромінювання в усіх типах блискавок локалізовані виключно всередині струмових шарів циліндричної форми. Запропоновано, що виміряне співвідношення між гальмівним та індукованим випромінюванням усередині струмового шару та поза його межами може слугувати критерієм геометричної локалізації джерела випромінювання. Відповідно до спостережень блискавок у вулканічних хмарах, спектри жорсткого випромінювання реєструються лише на їхній поверхні. Натомість наявність спектра жорсткого випромінювання у блискавках вулканічних хмар свідчить про їхню поверхневу локалізацію.

Ключові слова: *детектори жорсткого випромінювання, блискавка, радіаційне осадження, рентгенівська діагностика міцних прозорих вікон, дифузійне випромінювання, грозовий аерозоль.*